

Magnetic Domain Suppression in Fe/Si Multilayers with $^{11}\text{B}_4\text{C}$ Integration for Polarizing Neutron Optics

Anton Zubayer^{1,*}, Artur Glavic^{3,*}, Naureen Ghafoor¹, Yuqing Ge⁷, Yasmine Sassa⁷, Martin Månsson⁷, Andreas Suter³, Thomas Prokscha³, Zaher Salman³, Wai-Tung Lee⁴, Kristbjörg Anna Thórarinsdóttir², Arnaud Le Febvrier^{1,5}, Per Eklund^{1,5}, Jens Birch¹, Fridrik Magnus², Sean Langridge⁶, Andrew Caruana⁶, Christy Kinane⁶, Fredrik Eriksson^{1*}

Affiliations

¹Thin Film Physics Division, Department of Physics, Chemistry, and Biology (IFM), Linköping University, SE-581 83 Linköping, Sweden

²Science Institute, University of Iceland; Dunhaga 3, IS-107 Reykjavik, Iceland

³PSI Center for Neutron and Muon Sciences, 5232 Villigen PSI, Switzerland

⁴Science Directorate, European Spallation Source, Lund 224 84, Sweden

⁵Department of Chemistry-Ångström, Uppsala University; SE-75120, Uppsala, Sweden

⁶ISIS, Harwell Science and Innovation Campus, Science and Technology Facilities Council, Rutherford Appleton Laboratory, Didcot, Oxon OX11 0QX, United Kingdom

⁷Department of Applied Physics, KTH Royal Institute of Technology, SE-106 91 Stockholm, Sweden

*Corresponding authors, e-mail: anton.zubayer@liu.se, artur.glavic@psi.ch, fredrik.eriksson@liu.se

Abstract

This study explores the impact of boron carbide (B_4C) addition on magnetic domains within Fe/Si multilayers through off-specular neutron scattering with polarization analysis. The incorporation of B_4C induces amorphization in layers, disrupting magnetic domain structures. Analysis of the scattering patterns reveals that magnetic domains in pure Fe/Si multilayers exhibit no significant correlation between layers, resulting in a specific diffuse off-specular scattering signal, while the B_4C incorporated Fe/Si multilayers revealed no diffuse off-specular scattering. We offer a qualitative interpretation of these scattering phenomena and accurately model the observed diffuse patterns using the distorted wave Born approximation. Low-energy $\mu^+\text{SR}$ measurements further reveal that local magnetic fields in Fe/Si and Fe/Si + B_4C multilayers are more easily manipulated by external fields in B_4C -containing layers, with enhanced field uniformity in the muon length-scale. Our findings provide insights into the role of B_4C in altering magnetic domain arrangements within Fe/Si multilayers, contributing to advances in the design of magnetic materials and neutron polarization coatings.

Introduction

Magnetic domains in thin film multilayers are a key focus of research due to their critical role in magnetic behaviour and potential applications in spintronic devices and magnetic storage technologies. In systems like iron/silicon (Fe/Si) multilayers, the properties of magnetic domains are shaped by factors such as layer composition, thickness, and interface quality. Techniques such as magneto-optical Kerr effect (MOKE) microscopy, polarized neutron reflectometry (PNR), and X-ray magnetic circular dichroism (XMCD) have been widely used to explore domain patterns and magnetic anisotropy within individual layers.¹⁻³ Off-specular scattering, sensitive to lateral inhomogeneities and magnetic roughness, has emerged as a powerful tool to study domain structures and their evolution under different conditions. Recent investigations have explored how material modifications, such as introducing non-magnetic spacers or doping, influence domain formation

and stability.⁴ However, the impact of specific additives, such as boron carbide (B_4C), on magnetic domain behaviour in Fe/Si multilayers remains unclear. This study investigates how B_4C addition affects the magnetic domain structure in these systems.

The Fe/Si system and its magnetic domain configuration is of particular importance for application in coatings for neutron polarization devices. Polarizing neutron optics play a crucial role in neutron scattering experiments by enabling precise control and analysis of neutron spin states.⁵⁻⁹ High-quality polarizing optics are essential for improving the accuracy and sensitivity of measurements, which are fundamental in exploring the magnetic properties of materials in various fields such as condensed matter physics and materials science.¹⁰ To achieve this, polarizers are constructed as multilayered systems, typically composed of alternating magnetic and non-magnetic layers, designed to selectively reflect neutrons with a desired spin orientation.^{11,12} The difference in scattering contrast between spin-up and spin-down neutrons should be maximized to achieve enhanced polarization.^{13,14} This difference is directly related to the magnetization of the layers. To minimize the spin-down reflectivity, the neutron contrast for the non-magnetic layer must be well matched to the magnetic spin-down layer.

Several other factors, however, influence the polarization efficiency of such devices. The interface morphology becomes increasingly important for multilayers used at relatively large reflection angles to retain a high reflectivity.^{15,16} Furthermore, the formation of magnetic domains in the multilayer can lead to undesired spin-flip scattering that reduces polarization and may require high magnetic guide fields to be suppressed.^{17,18} The strength of this scattering depends on the magnetic domain sizes, the orientation of the local magnetization within a domain to the average magnetization, and the degree of correlation of domains between adjacent magnetic layers.

In previous studies, we have shown that incorporation of $^{11}B_4C$ into the multilayer system can improve interface quality and increase polarization of Fe/Si multilayers.⁴ This is achieved by amorphization of the Fe layers thereby suppressing roughness generated by crystallite facets at the interfaces. A secondary effect is that the magnetic coercivity of the sample is practically eliminated.

We employ neutron reflectometry and off-specular scattering with polarization analysis to investigate the magnetic domain patterns in Fe/Si multilayers with and without $^{11}B_4C$ incorporation. The focus is on the determination of approximate domain size and vertical domain correlations, as well as how the external magnetic field suppresses domain scattering. For ordinary Fe/Si structures we find small magnetic domains that show no interlayer correlations. We explain the scattering features and give a simple distorted wave Born approximation (DWBA) model that can reproduce the data. We show that by reducing or eliminating crystallinity, the incorporation of $^{11}B_4C$ effectively eliminates the magnetic domains, thereby mitigating magnetic off-specular scattering and improving the performance of polarizing neutron optics. In particular, the improvement in performance manifests itself by eliminating off-specular scattering, improving polarization performance and allowing the use of such coatings in applications where scattering from the optics is relevant. This technological improvement is advantageous for neutron optics, particularly for Small Angle Neutron Scattering (SANS) experiments, allowing for more detailed and accurate studies of material structures at the nanoscale.^{19,20}

We also employ low-energy μ^+SR (muon spin rotation) to probe the internal magnetic order within Fe/Si and Fe/Si + $^{11}B_4C$ multilayers. By tuning the stopping energies of the muons, we ensured implantation predominantly in either Fe or Si layers, allowing for detailed examination of local magnetic environments. The μ^+SR measurements were conducted under varying applied magnetic fields to observe the precession behavior and modulation of local fields. This approach provided valuable complementary insights into the magnetic response and tunability of the multilayers, particularly highlighting the enhanced field responsiveness in the B_4C -containing samples.

Experimental Details

Fe/Si and $^{11}\text{B}_4\text{C}$ -containing Fe/Si multilayer thin films were grown using ion-assisted DC magnetron sputter deposition in a ultra-high vacuum system, maintaining a background pressure of approximately 2×10^{-9} Torr (2.6×10^{-7} Pa). The details of the deposition system are described elsewhere.²¹ The multilayers were deposited onto $10 \times 10 \times 0.5$ mm³ Si (100) substrates with a native oxide layer, with the substrate held at ambient temperature (no intentional heating) and rotated at a constant speed of 15 rpm. The 50-mm-diameter sputtering targets were Fe (Plasmaterials, 99.95% purity), $^{11}\text{B}_4\text{C}$ (RHP Technology, 99.8% chemical purity, >90% isotopic purity), and Si (Kurt J. Lesker, 99.95% purity), operated at applied powers of 33 W, 50 W, and 20 W, respectively. Deposition rates were determined through X-ray reflectivity thickness measurements of the multilayers. The desired layer thicknesses and multilayer design were achieved using computer-controlled shutters, with opening durations tailored accordingly. During deposition, a DC substrate bias of -30 V was applied. In the case of Fe/Si + $^{11}\text{B}_4\text{C}$, each bilayer was formed by co-sputtering $^{11}\text{B}_4\text{C}$ with Fe, followed by the co-deposition of $^{11}\text{B}_4\text{C}$ with Si. The deposition rates for both Fe + $^{11}\text{B}_4\text{C}$ and Si + $^{11}\text{B}_4\text{C}$ were approximately 0.5 Å/s. The amount of $^{11}\text{B}_4\text{C}$ in the Fe and Si layers are 15 vol.% (or 15 atomic % of $^{11}\text{B} + \text{C}$). The 2 samples made for the XRR, XRD and PNR were Fe/Si and Fe/Si + $^{11}\text{B}_4\text{C}$ with 100 Å period thickness, a thickness ratio of 0.5 and 10 periods. While a second batch of the same materials Fe/Si and Fe/Si + $^{11}\text{B}_4\text{C}$ but with a period thickness of 500 Å and 2 periods, were made for the μ^+ SR experiments.

X-ray reflectivity (XRR) analysis was performed using a Panalytical Empyrean diffractometer configured in parallel beam geometry. The instrument utilized a line-focused Cu-K α (wavelength 1.54 Å) anode source which was operated at 45 kV and 40 mA. To condition the incident beam and limit the X-ray spot size on the sample, a parabolic X-ray mirror and a $\frac{1}{2}^\circ$ divergence slit were employed in the beam path. On the diffracted beam side, a parallel plate collimator with a 0.27° collimator slit was used, followed by a PIXcel detector operating in open detector mode. To analyze the XRR data, the multilayer period thickness and interface roughness were determined through a fitting process using the GenX software (v3.6.24).²²

X-ray diffraction (XRD) was conducted using a Panalytical X'Pert diffractometer configured in Bragg-Brentano geometry, with a Cu-K α (wavelength 1.54 Å). The setup included a Bragg-Brentano HD incident beam optics module equipped with a $\frac{1}{2}^\circ$ divergence slit and a $\frac{1}{2}^\circ$ anti-scatter slit. On the secondary optics side, a 5 mm anti-scatter slit was paired with an X'celerator detector operating in scanning line mode. Diffraction measurements were taken over a 2θ scanning range of 20° to 90° .

The magnetic properties of the samples were examined using vibrating sample magnetometry (VSM) on a quantum design PPMS,²³ in a longitudinal geometry at room temperature. Magnetic hysteresis curves were recorded over a field range of -20 mT to 20 mT, allowing for the visualization of the coercive field of the samples.

Polarized neutron reflectivity (PNR) and off-specular scattering with polarization analysis was performed at the POLREF beamline at the ISIS neutron and Muon Source in the UK.²⁴ The POLREF beamline is equipped with a front (incident beam) neutron polarizer and back end (reflected beam) neutron analyzer setups allowing the incident neutron spin eigenstate to be polarized and the reflected neutron spin eigenstate to be analyzed. This allows both the Non-spin Flip (NSF) and Spin Flip (SF) to be measured separately.²⁵⁻²⁷ The combination of NSF and SF measurements allows the magnitude and orientation of magnetization relative to the applied magnetic field to be measured as a function of depth through the sample. It is in essence a depth-dependent in-plane vector magnetometer. The off-specular analysis allows in-plane information to be measured within the length scale of a few 100 nm to 30 μm ²⁸⁻³¹ giving information on domain sizes, magnetic magnitude and orientation. Smaller domain sizes are limited by the accessible q_x -range while the neutron coherence (given by resolution) limits the largest accessible sizes. The samples were mounted in a room temperature bore GMW magnet capable of applying a uniform field of $\pm 0.7\text{T}$, which also defines the quantization axis for the neutron

polarization. The efficiencies of the polarization devices were corrected for with reference measurements following the method described by Wildes et al.³²

The BornAgain software³³ was employed to simulate both specular and off-specular neutron reflectivity in all four spin states using DWBA, thus including refraction and reflection effects. In combination with specular reflectivity refinements, these simulations allowed for the extraction of key structural and magnetic parameters of the Fe/Si and Fe/Si + ¹¹B₄C multilayers. Specifically, we obtained the layer thicknesses, interface roughnesses, magnetic domain sizes, and the orientation angles of the magnetic moments within the domains. The ability to model both the specular and off-specular scattering provided a comprehensive understanding of the magnetic structure and interlayer properties.

The Muon spin rotation (μ SR) experiment is performed at the low-energy μ SR spectrometer (LE- μ SR)³⁴ at the Swiss Muon Source (S μ S), Paul Scherrer Institute, Villigen, Switzerland. The data is analysed with the software musrfit.³⁵ The two samples were measured with external applied fields of 0, 1, 5 and 30 mT. The LE- μ SR time spectra are fitted with:

$$A_0 P_{TF}(t) = A_{B_0} \exp(-\lambda_{B_0} t) \cos(B_0 \gamma_\mu t) + A_S \exp(-\lambda_S t) + A_F \exp(-\lambda_F t) \quad 1$$

where the A_0 , A_{B_0} , A_S , and A_F are the total initial asymmetry, the initial asymmetry related to the local fields, and the slow and fast exponential relaxations, respectively. The λ_i s are the corresponding relaxation rates, the B_0 represents the average effective local fields muons experience in the sample as a result of the external fields combined with the internal fields from the magnetic order of the sample, and the $\gamma_\mu = 2\pi \times 0.01355 \text{ MHz/G}$ is the gyromagnetic ratio of the muon. The $B_{\text{ext}} = 0 \text{ mT}$ measurements were fitted assuming $A_{B_0} = 0$.

Results and Discussion

Magnetic off-specular scattering arises due to the presence of magnetic domains within the Fe layers. To distinguish general off-specular scattering from magnetic off-specular scattering, one must observe the behavior of the spin of scattered neutrons. If the off-specular scattering is magnetic in nature, the spin of the neutrons will flip after interacting with a magnetic domain (perpendicular deviation from the average moment) or a difference for spin-up and spin-down neutrons is observed (longitudinal deviation from average moment). This occurs because the magnetic moment within the domain is oriented differently from the applied external magnetic field and the layer averaged magnetization. Neutrons enter the multilayer structure and, upon encountering a magnetic domain within the Fe layer, may change their trajectory (scatter). The interaction with the magnetic domain also causes the neutrons to flip their spin.

In a multilayer structure the scattering is a complex combination of interference effects from waves reflected on all interfaces within the sample and the scattering within each layer that effect any of these waves. All these effects are considered in DWBA models. A qualitative explanation of the observed scattering patterns are depicted in Figure 1.

If the magnetic domains of adjacent magnetic layers are correlated (i.e. a magnetic coupling between layers exists) then the scattering amplitudes have a fixed phase relation that is equivalent with the relation between reflections from interfaces with the same distance. This leads to a strong off-specular signal at the same q_z -position as the multilayer Bragg-peak (a so-called Bragg-sheet depicted in Figure 1d). The fact that the optical parameters for spin-up and spin-down are different leads to an asymmetry between off-specular scattering to the different sides of the specular line for spin-flip channels. This asymmetry is inverted between up-down and down-up channels, which can be understood as an inversion of beam direction.

In the opposite case with no correlations between the magnetic domains of different layers, the scattering is added incoherently and no enhancement at the q_z of the Bragg-peak is observed. The incoming and outgoing beams, however, are still reflected on the sample interfaces. This means that there is not only a direct scattering from neutrons entering the sample towards the detector, the diffuse intensity which is strongest at low q close to the critical edge of total reflection (blue in Figure 1c), but also a possibility to reflect before or after the scattering process. For the Fe/Si system the spin-down contrast vanishes, and no Bragg-reflection is observed. Thus, the spin-up incident beam can make a Bragg-reflection and then scatter with spin-flip before leaving the sample freely (Figure 1a). The spin-down incident beam encounters the opposite effect, entering the sample freely before scattering and then being Bragg-reflected (Figure 1b). This situation leads to peculiar scattering patterns with triangular shape that are restricted by the critical angle on one side and a diagonal with $p_i/p_f = p_{\text{Bragg}}$ (green/red area marked with arrows in Figure 1c).

In this study, we employ a coordinate system wherein the out-of-plane momentum vector components p_i (initial) and p_f (final) are used as they match well to the observed off-specular scattering.^{30,36} The out-of-plane momentum transfer, denoted as q_z , is the sum of p_i and p_f , capturing correlations normal to the sample's surface. We define $p_{\text{Bragg}} = p_i = p_f = q_z/2$ at the superlattice specular Bragg peak. This choice facilitates the characterization of specular and off-specular scattering components, ensuring accurate quantification of scattering phenomena in relation to the Bragg condition.

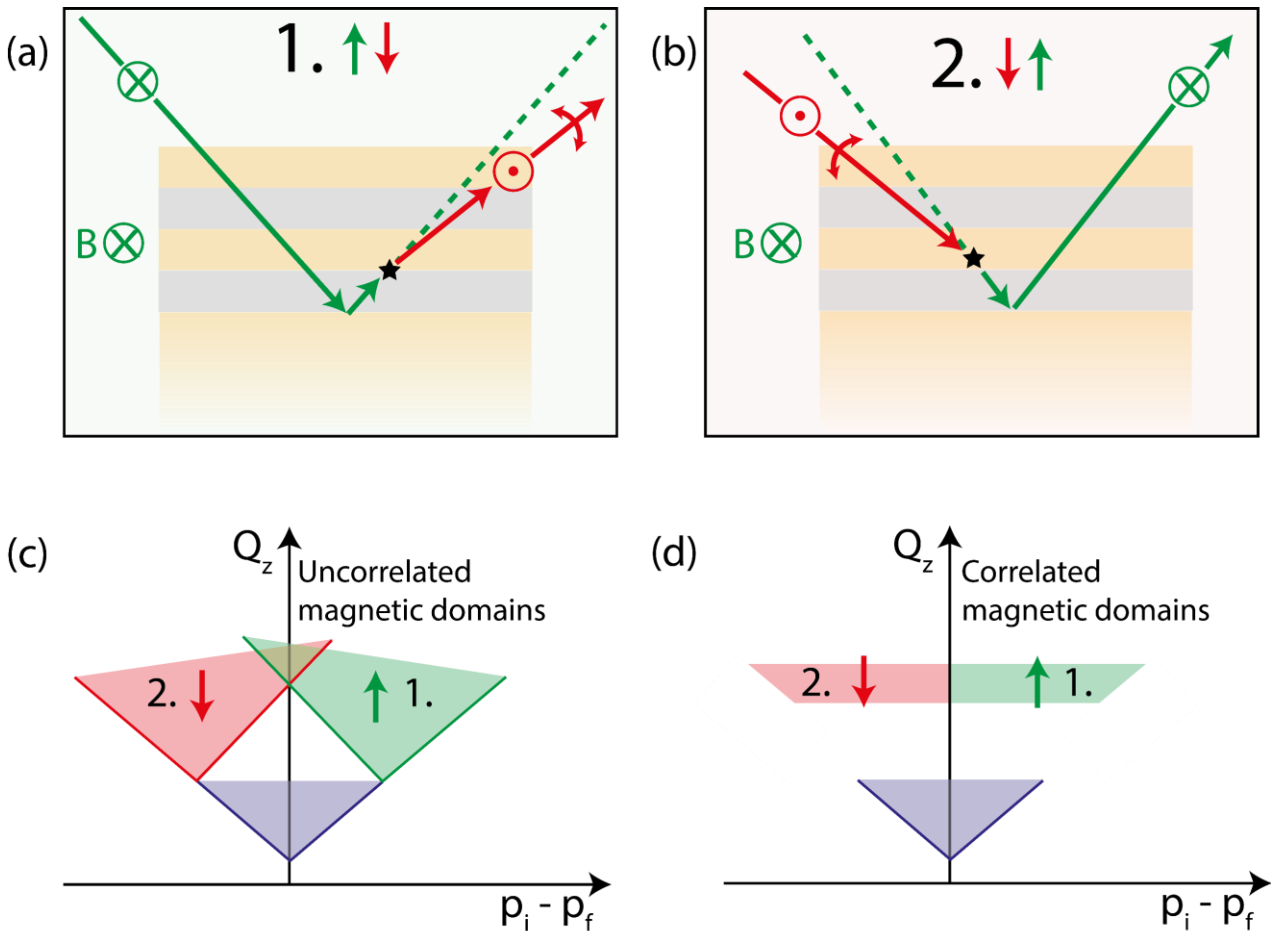


Figure 1. Sketch of the reason and shape of off-specular scattering patterns from magnetic domains; spin-up (a) or spin-down (b) neutrons entering a multilayer with uncorrelated domains. The applied external field, B , points into the paper. The star represents a point where the neutron is scattered on a magnetic domain in an Fe layer. In both cases the spin-up beam has enhanced reflectivity at the Bragg-peak. The bottom shows sketches of the resulting scattering patterns for vertically uncorrelated (c) and correlated (d) magnetic domains. In magnetic off-specular neutron scattering, p_i and p_f represent the components of the neutron wavevector along the surface normal for the incident and scattered beams,

respectively, and are crucial for determining the perpendicular momentum transfer Q_z , which is sensitive to variations in magnetic structures like domains or spin textures. In the Q_z vs p_i - p_f representation the specular reflectivity is vertical and Yoneda lines diagonal.

Two multilayers, Fe/Si and Fe/Si + $^{11}\text{B}_4\text{C}$ (co-sputter $^{11}\text{B}_4\text{C}$ with Fe and Si), were investigated. Each was designed to have a periodic thickness of $\Lambda = 100$ Å, a layer thickness ratio of $\Gamma = 0.5$, and a total of $N = 10$ periods. These multilayer parameters were selected to produce sufficient signal for the experiment while avoiding effects due to increasing roughness that would complicate the modelling.

XRR measurements and subsequent fitting using GenX3 reflectivity fitting software²² were performed to assess the multilayer parameters. In Figure 2(a), there is a significantly higher XRR reflectivity observed up to the 7th order Bragg reflection for the Fe/Si + $^{11}\text{B}_4\text{C}$ multilayer compared to the conventional Fe/Si multilayer. The simulated interface width for the Fe/Si + $^{11}\text{B}_4\text{C}$ multilayer is smaller, at $\sigma = 7.8$ Å, in contrast to the larger interface width of $\sigma = 11.5$ Å obtained for the low intensity peaks for the Fe/Si multilayer. The XRD analysis of the multilayers in Figure 2(b) shows that the multilayer that contains $^{11}\text{B}_4\text{C}$ is X-ray amorphous. In contrast, the pure Fe/Si sample exhibits crystallinity for Fe and possibly iron-silicide crystallites. The enhanced reflectivity, despite the reduced scattering length density (SLD) contrast between the layers due to the incorporation of $^{11}\text{B}_4\text{C}$ in both the Fe and Si layers, is therefore attributed to $^{11}\text{B}_4\text{C}$ induced amorphization and boron-metal bonding leading to smoother interfaces and reduced intermixing, respectively. Consequently, in agreement with our previous work, the reduced interface width contributes to the higher X-ray and neutron reflectivities.⁴

Furthermore, in agreement with our previous findings for thinner layers, the current multilayer with $\Lambda = 100$ Å also demonstrates no noticeable remanent magnetization and thus no coercivity in VSM measurements in $^{11}\text{B}_4\text{C}$ -containing multilayers, unlike the pure Fe/Si (Figure 2(c)).⁴ The lack of coercivity can be linked to the amorphous structure of the Fe/Si + $^{11}\text{B}_4\text{C}$ multilayer, which likely modifies the formation of magnetic domains due to the absence of crystalline anisotropy.¹⁷ Consequently, the absence of domains could facilitate easy magnetization as the material no longer exhibits the strong domain-related resistance characteristic of crystalline structures.³⁷

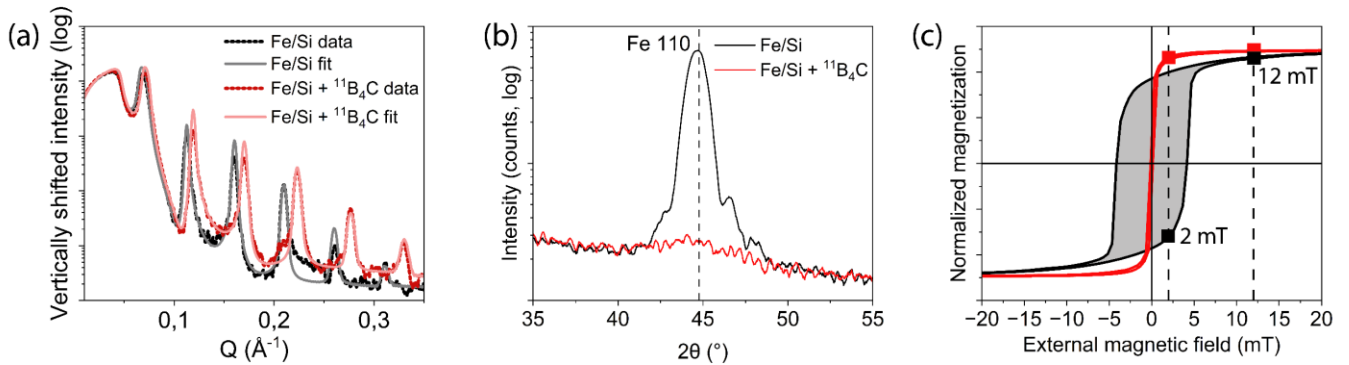


Figure 2. (a) X-ray reflectivity (XRR) with corresponding fits for the Fe/Si (black), and Fe/Si + $^{11}\text{B}_4\text{C}$ (red), samples.²² (b) X-ray diffraction (XRD) focusing on the angular region of 35-55°. (c) Vibrating sample magnetometry (VSM) with external fields between -20 and 20 mT. The magnetization is normalized to the saturation value. The red and black squared points represent the external fields used for measuring PNR for Fe/Si and Fe/Si + $^{11}\text{B}_4\text{C}$.

Figure 3 shows the results from the spin-flip off-specular neutron reflectivity measurements for Fe/Si to extract information on magnetic domain sizes and the degree of their rotation relative to the external magnetic field. The corresponding results for Fe/Si + $^{11}\text{B}_4\text{C}$ and additional data for other spin states and applied fields are shown in the supplemental information. Measurements were performed at external fields of 2 mT (Figure 3 (a-b)) and 12 mT (Figure 3 (c-d)). Additional measurements made at 700 mT for the Fe/Si sample are shown in S3(s-t). Whereas the experimental data already shows visual differences between the multilayers, the

corresponding simulations provide quantitative information on domain sizes and rotation angles. The key off-specular intensities of interest here are the spin-flip intensities, as they reveal the presence and behaviour of magnetic domains. When comparing the two multilayers, it is evident that the Fe/Si + $^{11}\text{B}_4\text{C}$ exhibits less, if any, off-specular scattering across any applied external magnetic fields, as seen in Figure 3(i-p). In contrast, the pure Fe/Si shows pronounced off-specular intensities, especially at 2 mT. This difference is consistent with the VSM results, which indicate that the Fe/Si is not magnetically saturated at 2 mT, while the $^{11}\text{B}_4\text{C}$ containing multilayer is nearly fully saturated. Notably, at 2 mT, the Fe/Si remains in a state of negative magnetization. Further, at 12 mT, where the coercive field has been passed, the Fe/Si still shows off-specular scattering. This observation is consistent with the observed incomplete saturation of magnetization.

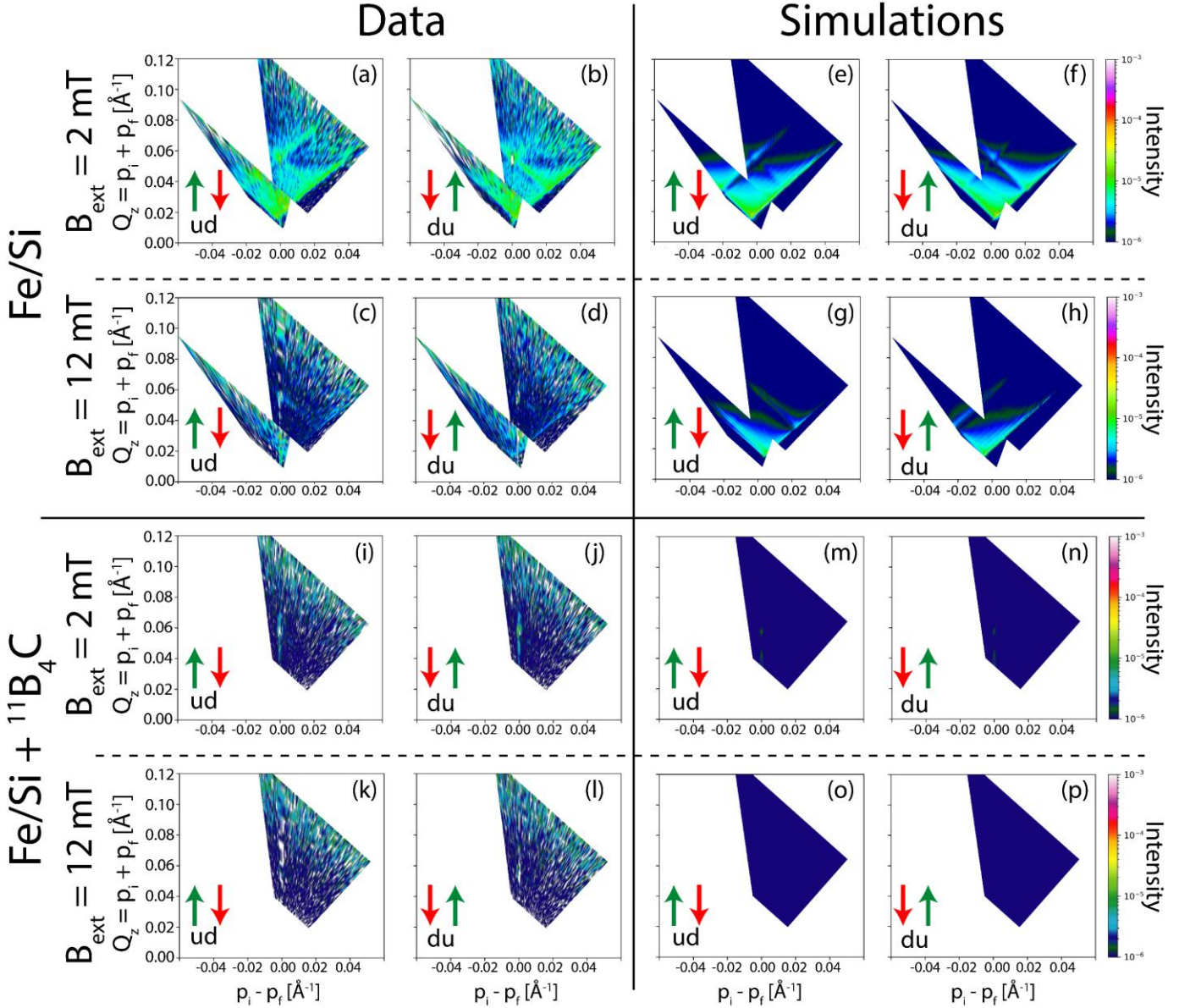


Figure 3. Spin-flip off-specular polarized neutron reflectivity (PNR) of Fe/Si. (a-b) showing the raw data for the 2 mT and (c-d) for 12 mT. While (e-f) shows the corresponding spin-flip off-specular simulations using BornAgain for 2 mT and (g-h) for 12 mT. (i-j) and (k-l) are the spin-flip off-specular PNR of Fe/Si + $^{11}\text{B}_4\text{C}$ measured at 2 and 12 mT external field respectively, while (m-n) and (o-p) shows the corresponding spin-flip off-specular simulations for 2 mT and (g-h) for 12 mT. All panels use a colour plot which indicates the neutron intensities in a log scale.

At 2 mT, the Fe/Si + $^{11}\text{B}_4\text{C}$ multilayer (Figure S5(c-d)) exhibits significantly less magnetic, and even non-magnetic, scattering compared to the pure Fe/Si multilayer at 12 mT (Figure S4(e-f)) and arguably even 700 mT (Figure S4(s-t)). This indicates that at very low field of 2 mT the $^{11}\text{B}_4\text{C}$ containing multilayer substantially

reduces magnetic domain-related scattering compared to the pure Fe/Si multilayer and minimizes off-specular scattering. The elimination of crystallinity in Fe/Si + $^{11}\text{B}_4\text{C}$ leading to the elimination of coercivity and more easy magnetic saturation, is directly linked to the absence of magnetic domains. This lack of domains effectively reduces off-specular scattering, as observed in the neutron reflectivity data.

The simulations in Figure 3(e-f) and Figure 3(g-h) use a model of uncorrelated magnetic domains in the Fe/Si sample, with domain sizes of 250 nm at 2 mT and an angle of 130° relative to the external field. At 12 mT, the domain size increases to 420 nm, and the angle decreases to 20° , indicating a shift towards greater alignment with the external magnetic field as the field strength increases. A schematic illustration based on these conclusions is visualized in Figure 5. The magnetic domains appear to have coalesced as the external field was increased from 2 mT to 12 mT. At 700 mT, the off-specular scattering in the Fe/Si sample is absent, indicating that the magnetic domains have fully aligned with the external magnetic field, effectively eliminating the scattering caused by domain misalignment. It should be noted that a magnetic field of 700 mT is significantly higher than the 40 mT typically used to operate polarizing neutron optics, making it impractical for most applications despite its ability to eliminate off-specular scattering caused by magnetic domains. Therefore, if a much lower field of only 2 mT can eliminate magnetic domains for Fe/Si + $^{11}\text{B}_4\text{C}$, this is a far more suitable option.

In Figure 4(a-b), the simulated specular reflectivity results from the BornAgain off-specular simulations provide key insights into the spin-up and spin-down reflectivity for the Fe/Si sample at 2 and 700 mT. The other magnetic fields and other sample, Fe/Si + $^{11}\text{B}_4\text{C}$, can be seen in the Supplementary. For the Fe/Si sample at 2 mT, the spin-down reflectivity is higher than the spin-up, which is attributed to the average magnetic moment pointing in the opposite direction to the external field. This effect is clearly seen in Figure 2(c), where 2 mT was insufficient to fully flip the magnetization. When comparing the reflectivity at 12 mT (Figure S1(b)) and 700 mT (Figure S1(c)) for Fe/Si, an improvement in polarization is observed at 700 mT, as the magnetization is fully saturated, unlike at 12 mT, which remains unsaturated as evidenced by the VSM data in Figure 2(c). In contrast, for the Fe/Si + $^{11}\text{B}_4\text{C}$ sample, no visible difference is observed between the reflectivity at 2 mT (Figure S1(d)) and 12 mT (Figure S1(e)), indicating faster magnetic saturation and the absence of magnetic domains. Figure 4(a), shows that the spin split is wider for the simulation (fit) compared to the experimental data. This could be attributed to the lower magnetic moment for the Fe-atoms in the Fe-layers compared to bulk value of Fe. The specular simulations of the other fields and other sample can be seen in Figure S2.

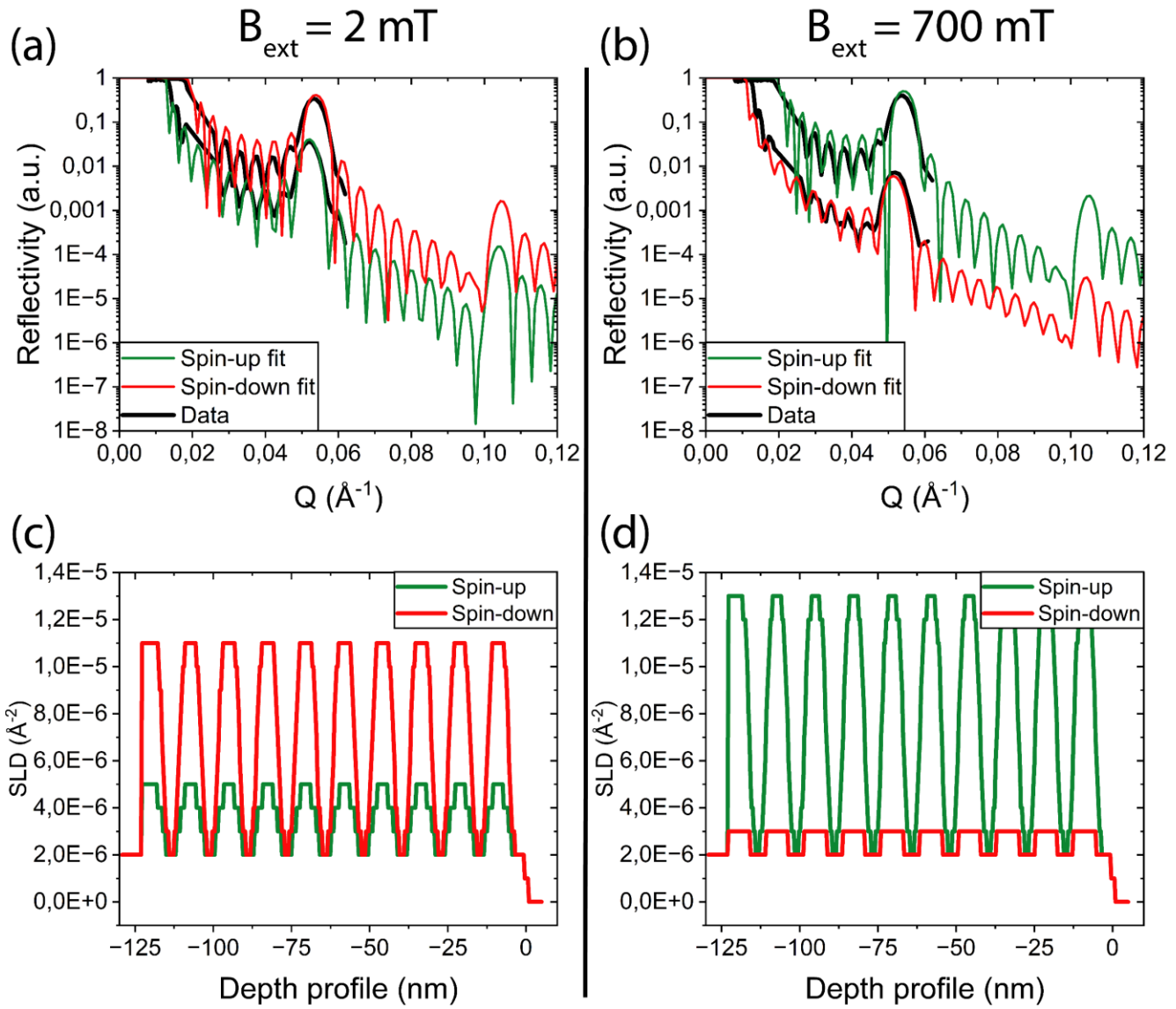


Figure 4. Specular PNR data is shown in (a-b) for 2 and 700 mT respectively (black), with specular simulations from the BornAgain software simulations (red/green) for corroboration of the experimental data. Polarized neutron reflectivity simulations taken from the BornAgain modelling software for the off-specular measurements corresponding to the experimental measurements. The simulation is of the Fe/Si at 2 mT (a) and 700 mT measurement in (b). The corresponding SLD profile is shown in (c) and (d), respectively, at different depths in the multilayer for the spin-up (green) and spin-down (red) case. 0 nm represents the surface of the film.

The corresponding spin-up and spin-down scattering length density (SLD) profiles from the simulations in Figure 4(c-d) and Figure S2 further illustrate the polarization behaviour at different magnetic field strengths. At 2 mT for the Fe/Si sample, the system is not well polarized, as indicated by both the incorrect polarization and poor contrast between the spin-up and spin-down SLD profiles. The profiles display a step-like pyramid structure for both spin orientations, a feature whose origin remains unclear but may suggest incomplete alignment of the magnetic domains with the external field. This poorly defined contrast and irregular SLD profile at 2 mT reflect the insufficient magnetic field to achieve proper polarization, consistent with the earlier observation that 2 mT is not strong enough to flip the magnetization fully in the Fe/Si system.

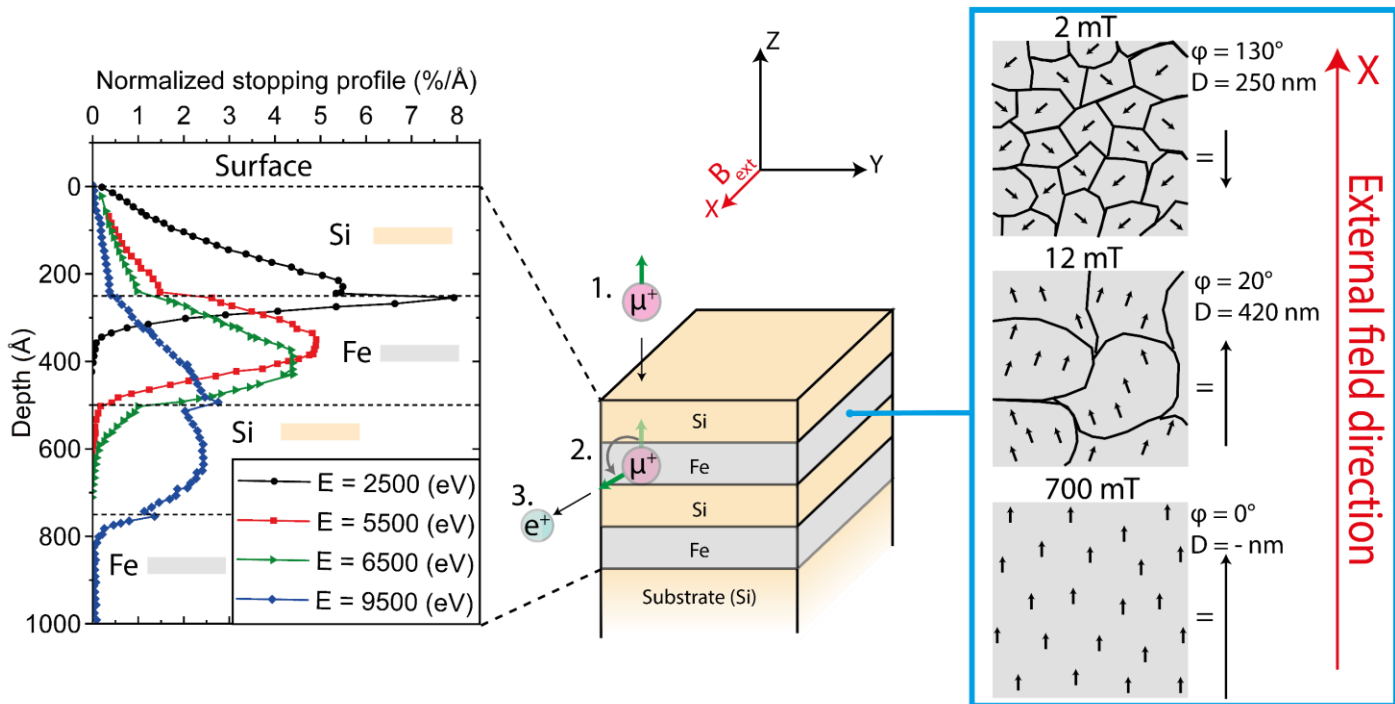


Figure 5. Schematic of the multilayer (center) along with the muon (μ^+) traversing towards it (1), implanting and precessing (2) and decaying into a positron (e^+), neutrino (ν_e) and antineutrino ($\bar{\nu}_e$) where the positron will eject in the direction of the muons last spin direction before decaying (3), before finally being captured by the detectors. The muon stopping profile is seen on the left where the muons are mainly implanted in different layers depending on their initial energy. The magnetic domains seen on the right (black domain boundaries) with their corresponding local alignment in relation to the external field (arrows inside the domains). The arrows to the right of the schematic domains show the net magnetization and the alignment with respect to the external field. The domain sketches, angle of canting (ϕ) and domain sizes (D) are results from the magnetic off-specular measurements and fitting.

A different model than the uncorrelated cylindric magnetic domains was also evaluated, to simulate the 4-spin state off-specular PNR. As shown in the supplement, the various correlated magnetic domain models fail to match the experimental data. Adjusting the domain size or shape and orientation did further diverging from experimental observations, too. We therefore conclude that the Fe/Si multilayer does exhibit uncorrelated magnetic domains with a typical size around 200 nm.

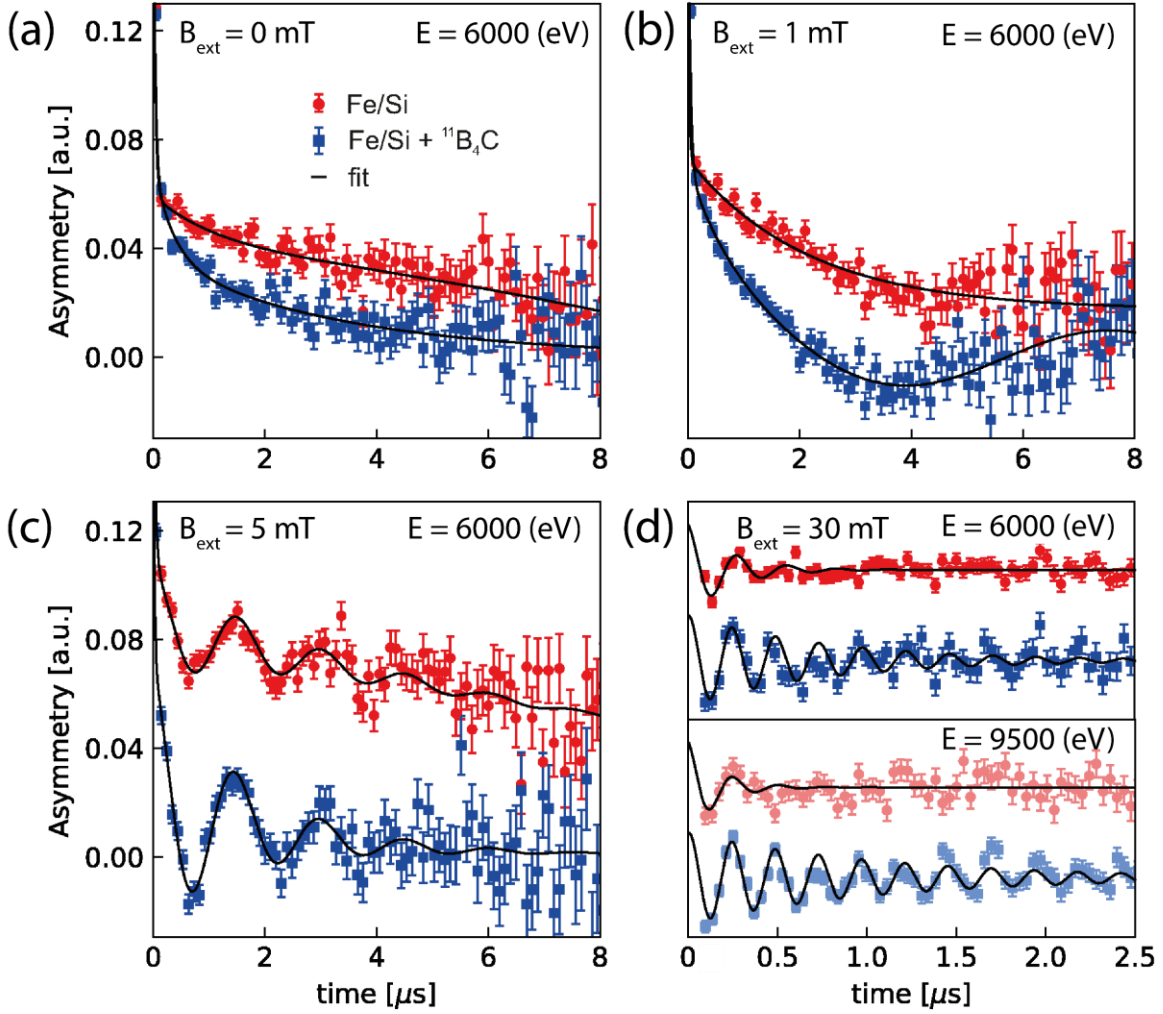


Figure 6. *LE- μ SR* time spectra obtained at various external fields applied parallel to the sample surface, at (a) 0 mT (b) 1 mT, (c) 5 mT, and (d) 30 mT. Spectra shown in (d) are the oscillation components normalized by the initial asymmetries of oscillation and shifted in the y-axis for clarity of view. The energy of 6000 eV corresponds to the majority of the muons implanted into the Fe layer, while with the 9500 keV muons are mostly in the Si layer. The sample has been saturated in an applied field of 55 mT in the opposite direction before (a-c) and (d) were carried out, separately. All measurements were carried out at room temperature. The red and blue data points represents the Fe/Si and Fe/Si + $^{11}\text{B}_4\text{C}$ sample respectively. The solid lines are fits corresponding to Equation (1).

To investigate the internal magnetic order in Fe/Si and Fe/Si + $^{11}\text{B}_4\text{C}$ multilayers, low energy μ^+ SR was performed on multilayers with the period thicknesses of 500 Å instead of 100 Å. These thicknesses were chosen due to the muon implanting stopping energies needed to make sure most of the muons would implant only in the first Fe or Si layer from the top. The energies of the muons are tuned to be mostly implanted in Fe layers and Si layers with energies of 6 keV and 9.5 keV, respectively. The fields are applied perpendicular (transverse) to the initial spins of the muons.

As seen in Figure 6, an applied field of 1 mT is large enough to induce a local field visibly manifesting the muon spin precession in the Fe/Si + $^{11}\text{B}_4\text{C}$ sample thereby a cosine oscillation can be seen in the spectrum, while no substantial oscillation of comparable magnitude can be seen in the Fe/Si sample. The presence of the oscillation with a frequency corresponding to the external field in the Fe/Si + $^{11}\text{B}_4\text{C}$ sample indicates that the local magnetic environment inside the Fe layer can be well modulated by an external field of 1 mT. Upon increasing the applied field, such kind of oscillations start to be present in both samples. However, the

oscillations are much less relaxed and long-persisting in the $^{11}\text{B}_4\text{C}$ containing layers, especially at an external field of 30 mT with relaxation rates $\lambda_{B_0} = 2.1(8)/\mu\text{s}$ for the Fe/Si + $^{11}\text{B}_4\text{C}$, but a $\lambda_{B_0} = 5.1(9)/\mu\text{s}$ for the Fe/Si. In the spectra, the oscillations of the best fits persist for more than 2.5 μs in the Fe/Si + $^{11}\text{B}_4\text{C}$ sample, while only up to 2 cycles of the cosine functions are present in the Fe/Si. $\mu^+\text{SR}$ serves as a local probe, providing unique insights into the uniformity of the local magnetic environment at the muon stopping site. While bulk-averaged (VSM) and long-range (PNR) techniques highlight the macroscopic effects of $^{11}\text{B}_4\text{C}$ inclusion, the LEM results reveal that this effect persists even at the muon length-scale. Here we refer the muon length-scale using LE- $\mu^+\text{SR}$ to a few nanometres.³⁸ The observed oscillating asymmetries in the Fe/Si + $^{11}\text{B}_4\text{C}$ sample, along with the possible absence of multiple frequencies in the spectra, suggest no phase separation at the local level and confirm the single-domain-like behavior. The reduced relaxation rates and longer-persisting oscillations in the $^{11}\text{B}_4\text{C}$ -containing sample further indicate that the inclusion of $^{11}\text{B}_4\text{C}$ enhances the uniformity of local magnetic fields. This consistency across bulk, long-range, and local probes demonstrates that the favorable magnetic properties of $^{11}\text{B}_4\text{C}$ -containing multilayers arise from its stabilizing effect on the local magnetic environment.

Conclusions

We have examined the effect of $^{11}\text{B}_4\text{C}$ on the magnetic domain structure of Fe/Si multilayers and how it improves polarizing neutron optics. For situations with significant off-specular scattering we could build a quantitative model using DWBA as well as give an intuitive explanation of the scattering process. This understanding can be applied generically to any magnetic multilayer to interpret the scattering pattern and distinguish between correlated and uncorrelated magnetic structures.

In Fe/Si multilayers, magnetic domains were identified with sizes of approximately 250 nm at 2 mT and 420 nm at 12 mT, with significant canting to the external field. At 700 mT, off-specular scattering disappears, indicating a homogeneous magnetization. In contrast, the Fe/Si + $^{11}\text{B}_4\text{C}$ multilayer (co-sputter $^{11}\text{B}_4\text{C}$ with Fe and Si) showed no off-specular scattering at any field, suggesting the elimination of magnetic domains due to $^{11}\text{B}_4\text{C}$ -induced amorphization, which reduces coercivity and allows easier magnetic saturation. Low-energy $\mu^+\text{SR}$ measurements further corroborated these findings by revealing that local magnetic fields within the Fe/Si + $^{11}\text{B}_4\text{C}$ multilayers are not only more uniform but also highly responsive to external fields, with possibly no phase separation at the muon length scale. This highlights the consistent behavior across bulk (VSM), long-range (PNR), and local ($\mu^+\text{SR}$) probes, confirming the stabilizing effect of $^{11}\text{B}_4\text{C}$ on the magnetic environment. The elimination of magnetic domains and reduced off-specular scattering in $^{11}\text{B}_4\text{C}$ -containing multilayers can result in improved performance of neutron polarizing devices, enabling more accurate measurements and requiring a lower external magnetic field for operation, thereby offering greater versatility in the design of polarizing neutron optics. These improvements make $^{11}\text{B}_4\text{C}$ an attractive additive to Fe/Si multilayers for improving the performance and reliability of neutron scattering experiments, for example as transmission analyzers for Small Angle Neutron Scattering (SANS) experiments. Other applications of magnetic thin films and nano-structures, where low coercivity is desired, could also benefit from this technology.

Acknowledgements

We would like to thank the ISIS neutron source of the provision of beamtime (RB2310605). The ISIS data is available at the following DOI <https://doi.org/10.5286/ISIS.E.RB2310605-1>. This work was supported by the Swedish Research Council (VR), grant number 2019-04837_VR. A.Z acknowledge the grant 2022-D-03 from the Hans Werthén Foundation, the grant from Royal Swedish Academy of Sciences Physics grant, PH2022-0029, the Lars Hiertas Minne foundation grant FO2022-0273 and the Längmannska Kulturfonden grant BA23-1664. MM acknowledge funding from the Swedish Research Council, VR (Dnr. 2021-06157 and Dnr. 2022-03936), the Swedish Foundation for Strategic Research (SSF) within the Swedish national graduate

school in neutron scattering (SwedNess), and the Carl Tryggers Foundation for Scientific Research (CTS-22:2374). Y.S. acknowledge funding from the Knut and Alice Wallenberg Foundation through the grant 2021.0150. Y.G. acknowledge funding from the KTH Royal Institute of Technology, Materials Platform. The μ SR experiments were performed at the Swiss Muon Source $S\mu S$, Paul Scherrer Institute, Villigen, Switzerland. We highly appreciate the great technical and scientific support from the local staff.

References

1. Yu, C., Jiang, H., Shen, L., Flanders, P. & Mankey, G. The magnetic anisotropy and domain structure of permalloy antidot arrays. *J. Appl. Phys.* **87**, 6322–6328 (2000).
2. Kudo, K. *et al.* Simulations of magnetic domain patterns on the surface of Co/Ni multilayers. *Surf. Interface Anal.* **46**, 962–969 (2014).
3. Welp, U., Vlasko-Vlasov, V., Liu, X., Furdyna, J. & Wojtowicz, T. Magnetic domain structure and magnetic anisotropy in Ga_{1-x}Mn(x)As. *Phys. Rev. Lett.* **90**, 167206 (2003).
4. Zubayer, A. *et al.* Reflective , polarizing , and magnetically soft amorphous neutron optics with 11B enriched B4C. *Sci. Adv.* **0402**, 1–7 (2024).
5. Kulda, J. *et al.* Neutron optics of the ILL high-flux polarized neutron three-axis spectrometer IN20B. *Proc. SPIE* (2001) doi:10.1117/12.448071.
6. Gubarev, M., Ramsey, B. & Mildner, D. Grazing-Incidence Neutron Optics based on Wolter Geometries. *Proc. SPIE* (2008).
7. Shimizu, H. Applications of Neutron Optics. *HAMON* (1991) doi:10.5611/HAMON.14.63.
8. Krist, T. Trevor Hicks and solid state neutron optics. *J. Phys. Condens. Matter* (2009) doi:10.1088/0953-8984/21/12/124208.
9. Mildner, D., Chen, H., Downing, R. G., Benenson, R. E. & Glinka, C. Low-resolution small-angle scattering using neutron focusing optics. *J. Phys. IV* (1993) doi:10.1051/JP4:1993889.
10. Garlea, O. *et al.* VERDI: VERsatile DIffractometer with wide-angle polarization analysis for magnetic structure studies in powders and single crystals. *Rev. Sci. Instrum.* (2022) doi:10.1063/5.0090919.
11. Peskov, B., Pleshanov, N., Pusenkov, V. & Syromyatnikov, V. NEUTRON OPTICAL DEVICES OF PNPI. *Proc. PNPI*.
12. Schreyer, A. *et al.* Spin polarized neutron reflectivity study of a Co/Cu superlattice. *J. Appl. Phys.* (1993) doi:10.1063/1.353958.
13. Majkrzak, C. F. & Berk, N. F. Neutron flux enhancement using spin-dependent interaction potentials. *Phys. Rev. B* **40**, 371 (1989).
14. Heinemann, A. & Wiedenmann, A. Benefits of polarized small-angle neutron scattering on magnetic nanometer scale structure modeling. *J. Appl. Crystallogr.* **36**, 1296–1302 (2003).
15. Eymery, J., Hartmann, J. & Baumbach, G. Interface dilution and morphology of CdTe/MnTe superlattices studied by small- and large-angle x-ray scattering. *J. Appl. Phys.* **87**, 3723–3731 (2000).
16. Fragneto, G. & Menelle, A. Progress in neutron reflectometry instrumentation. *Eur. Phys. J. Plus* **126**, 110 (2011).
17. Paul, A., Kentzinger, E., Rucker, U., Bürgler, D. & Brückel, T. Field-dependent magnetic domain

- structure in antiferromagnetically coupled multilayers by polarized neutron scattering. *Phys. Rev. B* **73**, 94441 (2006).
18. Sato, T. *et al.* Neutron-depolarization analysis and small-angle neutron-scattering studies of the reentrant spin glass Ni₇₇Mn₂₃. *Phys. Rev. B* **48**, 6074 (1993).
 19. Alefeld, B., Fabian, H. & Springer, T. Recent Studies In Neutron Optics, In Particular For Small-Angle Neutron Scattering. in *Proceedings of SPIE* vol. 1149 9–14 (1989).
 20. Mildner, D., Hammouda, B. & Kline, S. A refractive focusing lens system for small-angle neutron scattering. *J. Appl. Crystallogr.* **38**, 933–939 (2005).
 21. le Febvrier, A. *et al.* An upgraded ultra-high vacuum magnetron-sputtering system for high-versatility and software-controlled deposition. *Vacuum* **187**, (2021).
 22. Glavic, A. & Björck, M. GenX 3: The latest generation of an established tool. *J. Appl. Crystallogr.* **55**, 1063–1071 (2022).
 23. Design, Q. Physical Property Measurement System (PPMS): EverCool II cryogen-free refrigerator. (2024).
 24. Polref Instrument Overview.
 25. Moon, R. M., Riste, T. & Koehler, W. C. Polarization analysis of thermal-neutron scattering. *Phys. Rev.* **181**, 920–931 (1969).
 26. Blundell, S. J. & Schofield, A. J. Neutron polarization analysis in magnetism. *J. Magn. Magn. Mater.* **121**, 185–188 (1993).
 27. Blundell, S. J. & Schofield, A. J. Polarized neutron diffraction of magnetic structures. *Phys. Rev. B* **46**, 3391–3400 (1992).
 28. Majkrzak, C. F. & O'Donovan, K. V. Phase-sensitive neutron scattering in thin magnetic films. *Phys. Rev. A* **89**, 33851 (2014).
 29. Majkrzak, C. F., Berk, N. F. & Maranville, B. B. Neutron reflectometry for materials science. *J. Appl. Crystallogr.* **55**, 787–812 (2022).
 30. Ott, F. & Kozhevnikov, S. Off-specular data representations in neutron reflectivity. *J. Appl. Crystallogr.* **44**, 359–369 (2011).
 31. Dorner, B. & Wildes, A. R. Some considerations on resolution and coherence length in reflectometry. *Langmuir* **19**, 7823–7828 (2003).
 32. Wildes, A. R. Scientific Reviews: Neutron Polarization Analysis Corrections Made Easy. <https://doi.org/10.1080/10448630600668738> **17**, 17–25 (2007).
 33. Pospelov, G. *et al.* BornAgain: software for simulating and fitting grazing-incidence small-angle scattering. *J. Appl. Crystallogr.* **53**, 262–276 (2020).
 34. Prokscha, T. *et al.* The new μ E 4 beam at PSI: A hybrid-type large acceptance channel for the generation of a high intensity surface-muon beam. *Nucl. Instruments Methods Phys. Res. Sect. A Accel. Spectrometers, Detect. Assoc. Equip.* **595**, 317–331 (2008).
 35. Suter, A. & Wojek, B. M. Musrfit: A Free Platform-Independent Framework for μ sR Data Analysis. *Phys. Procedia* **30**, 69–73 (2012).
 36. Lauter, V., Lauter, H. J. C., Glavic, A. & Toperverg, B. P. *Reflectivity, Off-Specular Scattering, and GISANS Neutrons. Reference Module in Materials Science and Materials Engineering* (Elsevier Ltd., 2016). doi:10.1016/b978-0-12-803581-8.01324-2.
 37. Frackowiak, Ł. *et al.* Magnetic Domains without Domain Walls: A Unique Effect of He⁺ Ion

Bombardment in Ferrimagnetic Tb/Co Films. *Phys. Rev. Lett.* **124**, 47203 (2019).

38. Jackson, T. J. *et al.* Depth-Resolved Profile of the Magnetic Field beneath the Surface of a Superconductor with a Few nm Resolution. *Phys. Rev. Lett.* **84**, 4958–4961 (2000).